NEUROSCIENCE

Mass spectrometry imaging identifies abnormally elevated brain L-DOPA levels and extrastriatal monoaminergic dysregulation in L-DOPA–induced dyskinesia

Elva Fridjonsdottir[1], Reza Shariatgorji[1,2], Anna Nilsson[1,2], Theodosia Vallianatou[1], Luke R. Odell[3], Luke S. Schembri[1,2], Per Svenningsson[4], Pierre-Olivier Fernagut[5,6,7], Alan R. Crossman[8], Erwan Bezard[5,6,9]*, Per E. Andrén[1,2]*

L-DOPA treatment for Parkinson's disease frequently leads to dyskinesias, the pathophysiology of which is poorly understood. We used MALDI-MSI to map the distribution of L-DOPA and monoaminergic pathways in brains of dyskinetic and nondyskinetic primates. We report elevated levels of L-DOPA, and its metabolite 3-*O*-methyldopa, in all measured brain regions of dyskinetic animals and increases in dopamine and metabolites in all regions analyzed except the striatum. In dyskinesia, dopamine levels correlated well with L-DOPA levels in extrastriatal regions, such as hippocampus, amygdala, bed nucleus of the stria terminalis, and cortical areas, but not in the striatum. Our results demonstrate that L-DOPA–induced dyskinesia is linked to a dysregulation of L-DOPA metabolism throughout the brain. The inability of extrastriatal brain areas to regulate the formation of dopamine during L-DOPA treatment introduces the potential of dopamine or even L-DOPA itself to modulate neuronal signaling widely across the brain, resulting in unwanted side effects.

INTRODUCTION

Since its introduction for the treatment of Parkinson's disease (PD), L-3,4-dihydroxyphenylalanine (L-DOPA) remains the most effective therapy for alleviating parkinsonian symptoms. The therapeutic effects of L-DOPA are assumed to rely upon its conversion into dopamine (DA) following decarboxylation by the enzyme aromatic L-amino acid decarboxylase (AADC). Although highly effective in the early stages of PD, long-term treatment leads to abnormal involuntary movements or L-DOPA–induced dyskinesia (LID) that affects 10% of patients per year of treatment (*1*). LID represents the most debilitating motor side effect of DA replacement therapy and markedly reduces the clinical benefit of L-DOPA treatment. The current pathophysiological hypothesis of LID involves pulsatile stimulation of DA receptors, large fluctuations in extracellular concentrations of DA and L-DOPA in the striatum, abnormal signaling downstream of DA synapses, and changes in nondopaminergic neurotransmitter systems (*2*–*4*). In particular, the 5-hydroxytryptamine (5-HT) system has been implicated in dyskinesia. It has been shown that 5-HT neurons may release DA as a false neurotransmitter during L-DOPA treatment (*5*–*8*). In addition, by targeting the 5-HT system, dyskinesia has been alleviated in both preclinical and clinical studies (*2*). These alterations disrupt striatal information integration leading to abnormal basal ganglia output, resulting in hyperkinetic movements or dyskinesia (*4*).

Several lines of evidence suggest that LID is associated not only with striatal fluctuation in DA but also with widespread dysregulation of monoaminergic system homeostasis, involving both motor and nonmotor circuits within and outside the basal ganglia (*9*, *10*). Such changes may occur when L-DOPA is taken up by nondopaminergic neurons containing AADC and converted to DA, which may, in turn, affect the synaptic concentration and signaling of other neurotransmitters (*11*). Besides contributing to LID, such alteration may also be involved in L-DOPA–induced nonmotor fluctuations (*4*). The precise nature and extent of these neurochemical alterations remain poorly understood. We took advantage of matrix-assisted laser desorption/ionization mass spectrometry imaging (MALDI-MSI) to comprehensively map monoaminergic changes in the brain of a nonhuman primate model of PD.

Advances in the field of MSI have established the great potential of the technique in neuroscience through its ability to detect a wide range of neuroactive compounds and metabolites in a single tissue section (*12*, *13*). It measures the tissue levels of endogenous compounds, at a specific time point, where a single experiment can produce thousands of molecular images, displaying their quantitative tissue distribution (*14*). Here, we apply a recently developed method using ultrahigh mass resolution Fourier transform ion cyclotron resonance (FTICR) MALDI-MSI to map multiple neurotransmitters and downstream metabolites, including catecholaminergic, serotoninergic, and γ-aminobutyric acid (GABA)-ergic pathways using a derivatization approach targeting primary amines and phenolic hydroxyl groups to facilitate the ionization of the neurotransmitter metabolic pathways (*15*).

Samples from a previously published brain biobank of 1-methyl-4-phenyl-1,2,3,6-tetrahydropyridine (MPTP)–exposed nonhuman primate model of PD were investigated (*16*–*18*). This model is

[1]Medical Mass Spectrometry Imaging, Department of Pharmaceutical Biosciences, Uppsala University, Uppsala, Sweden. [2]Science for Life Laboratory, National Resource for Mass Spectrometry Imaging, Uppsala University, Uppsala, Sweden. [3]Department of Medicinal Chemistry, Uppsala University, Uppsala, Sweden. [4]Section of Neurology, Department of Clinical Neuroscience, Karolinska Institutet, Stockholm, Sweden. [5]Université de Bordeaux, Institut des Maladies Neurodégénératives, Bordeaux, France. [6]CNRS, Institut des Maladies Neurodégénératives, Bordeaux, France. [7]Université de Poitiers, INSERM, U0-1084, Laboratoire de Neurosciences Expérimentales et Cliniques, Poitiers, France. [8]University of Manchester, Manchester M13 9PL, UK. [9]Motac Neuroscience, Manchester M15 6WE, UK.
*Corresponding author. Email: erwan.bezard@u-bordeaux.fr (E.B.); per.andren@farmbio.uu.se (P.E.A.)

considered to be the optimal model to study preclinical LID, as it mimics well the human representation of the disease (*19*). We investigated neurochemical changes between untreated control animals, animals receiving MPTP without L-DOPA (MPTP), MPTP-administered animals with chronic L-DOPA treatment but without dyskinesia (non-LID), and MPTP-administered animals with chronic L-DOPA treatment displaying dyskinesia (LID). We thoroughly compared the non-LID and LID groups to quantify the extent of dysregulation of monoaminergic metabolism occurring in dyskinesia without the interference of changes that may arise due to MPTP administration. Neurotransmitter and metabolite levels were quantified in coronal tissue sections, enabling investigation of molecular tissue distribution in 18 brain regions. In addition, we performed a qualitative comparison of tissue distribution of neurotransmitters between the groups in selected brain regions and explored the potential of the method for showing the DA displacement in 5-HT neurons by comparing the distribution of these two neurotransmitters.

RESULTS

Animal behavioral data

The brain tissues analyzed in the current study were obtained from a previously published biobank, which contains untreated controls, parkinsonian MPTP-exposed without L-DOPA treatment (MPTP), L-DOPA–treated nondyskinetic parkinsonian (non-LID), and L-DOPA–treated dyskinetic parkinsonian (LID) rhesus monkeys (*16*–*18*). Parkinsonism exhibited by MPTP (disability score = 8.5 ± 0.5), non-LID (disability score = 9.8 ± 2.1), and LID groups (disability score = 9.3 ± 2.1) was fully comparable and directly related to the extent of lesion of DA terminals in the striatum in comparison to controls as evidenced by (i) in vivo binding of [^{99m}Tc]TRODAT-1, a DA transporter marker, using single-photon emission computed tomography (*18*), (ii) ex vivo DA transporter binding autoradiography using [^{125}I]PE2I (>95%) (*18*), (iii) counting of tyrosine hydroxylase (TH)–immunopositive neurons in the substantia nigra pars compacta (>80%) (*20*), (iv) measurement of DA levels by high-performance liquid chromatography (HPLC) (>92%) (*9*), and (v) detailed high-resolution analysis of TH and DA transporter-immunopositive DA fibers in the striatum (*20*).

Despite the comparable extent of lesions and of the L-DOPA dose administered to non-LID and LID animals, non-LID animals had no dyskinesia (dyskinesia score = 0), while LID animals experienced an average peak dyskinesia rating of 2.3 ± 0.5. After oral administration of the fixed dose of L-DOPA, both non-LID and LID animals exhibited similar reversal of their parkinsonism, an effect peaking from 30 to 40 min after administration until 150 to 180 min, before progressively returning to the OFF state as classically observed (*17*, *21*–*24*). Dyskinesia in the LID group peaked from 50 to 60 min after L-DOPA intake until 130 to 150 min, as previously reported (*17*, *21*–*24*).

Peripheral and brain bioavailability of L-DOPA

Both L-DOPA–treated groups received one last L-DOPA dose 1 hour before euthanasia, i.e., at the peak of antiparkinsonian and prodyskinetic effects (*16*–*18*). L-DOPA levels were assessed, at 1 hour after administration, in the plasma and cerebrospinal fluid (CSF) of separate (but concomitantly prepared) groups of non-LID (n = 4; PD score = 8.9 ± 1.8; LID score = 0) and LID monkeys (n = 4: PD score = 9.2 ± 1.7; LID score = 2.5 ± 0.7). L-DOPA levels were indistinguishable between the two groups both in plasma (non-LID, 6.963 ± 1.729 μg/ml; LID, 7.645 ± 1.262 μg/ml, P = 0.54) and in CSF (non-LID, 0.161 ± 0.060 μg/ml; LID, 0.176 ± 0.031 μg/ml, P = 0.66). Slopes of the linear regression (LR) traced from the correlation between CSF and plasma concentrations were identical in the two conditions (non-LID, R^2 = 0.76; LID, R^2 = 0.83), suggesting that brain bioavailability of L-DOPA was identical in both non-LID and LID groups.

DA distribution in tissue sections from control, MPTP, LID, and non-LID animals

DA distribution was visualized in the post-commissural striatum of controls, MPTP, non-LID, and LID animals (Fig. 1, A and B). The MALDI-MS images show decreased levels of DA as a result of the degeneration of dopaminergic neurons, leading to a loss of terminals in the putamen (Put) and caudate nucleus (Cd), following MPTP exposure, as expected in this model (*18*, *25*). The untreated controls had high levels and a relatively homogeneous distribution of DA throughout the Cd and Put (Fig. 1A). Following MPTP exposure, the remaining DA was mostly located in the dorsomedial part of the Put, with round patches displaying high levels of DA distributed throughout the striatum. A similar pattern was observed for the non-LID and LID animals, although the LID animals showed a lower number of DA patches in the Put (Fig. 1B). The control group had significantly higher DA in Cd and Put than the other groups (Fig. 1C). The LID animals did not significantly differ from MPTP and non-LID groups, although there was a nonsignificant trend of increased DA in striatal structures (Fig. 1C), which may have arisen from high variance of DA levels in the LID group and the relatively small number of animals.

Both segments of globus pallidus (GP) had a trend of decreased DA in the MPTP and non-LID groups, whereas the LID group had an increased level of DA, comparable to the control group (Fig. 1C). The LID group had higher DA than control and MPTP groups in the precentral gyrus (PrG), where the motor cortex is located. The thalamus and the amygdala did not show significant change. DA was, however, increased in the hypothalamus and the hippocampus in the LID animals compared to the other three groups. DA was slightly higher in the bed nucleus of stria terminalis (StT) in the LID animals compared to MPTP animals.

MALDI-MSI of multiple neurotransmitters and metabolites

Fourteen neurotransmitters and metabolites were simultaneously imaged and identified with accurate mass (table S1). MS/MS was used to further confirm the identity of DA, L-DOPA, 3-*O*-methyldopa (3-OMD), 3-methoxytyramine (3-MT), norepinephrine (NE), 5-HT, 5-hydroxyindolic acid (5-HIAA), and GABA (fig. S1). MS imaging provides an additional parameter for identification purposes over traditional MS, namely, anatomical distribution, which was used to further confirm the identifications. In addition, the number of reactive sites for derivatization (primary amines and phenolic hydroxy groups) on the analytes of interest was used for identification (fig. S1 and table S1), as described previously (*15*). The identified metabolites included eight components of the catecholamine metabolic pathway, i.e., L-DOPA, DA, 3-MT, 3,4-dihydroxyphenylacetic acid (DOPAC), homovanillic acid (HVA), NE, 3,4-dihydroxy-phenylglycol (DOPEG), and 3-methoxy-4-hydroxyphenylglycol (MOPEG), and also the main metabolite of L-DOPA formed during pharmacological treatment, 3-OMD (fig. S2). 5-HT and its metabolites 5-hydroxyindoleacetic acid (5-HIAL) and 5-HIAA were imaged, in addition to taurine and GABA (fig. S2).

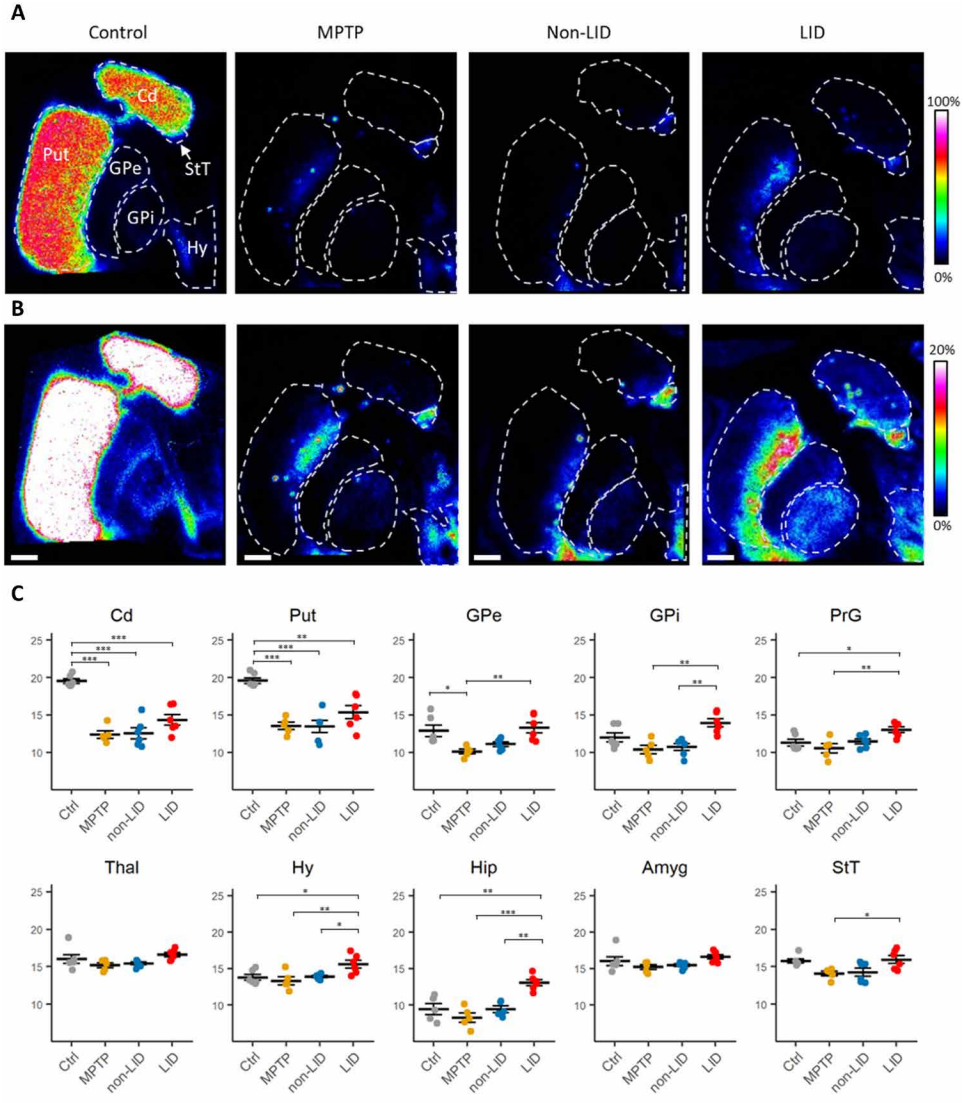

Fig. 1. Tissue distribution of DA in basal ganglia structures and regional quantitation of DA. DA distribution in basal ganglia structures in (**A**) control, MPTP, non-LID, and LID tissue sections, scaled to 0 to 100% of maximum intensity and (**B**) to 0 to 20% of maximum intensity. Lateral resolution, 80 μm; all images are log-transformed and RMS-normalized; scale bars, 4 mm. Coronal level, −4 mm ac. (**C**) Regional quantitation of DA; *y* axis shows $\log_2$AUC of DA. $n = 6$ for Ctrl, non-LID, and LID; $n = 5$ for MPTP. A two-way ANOVA followed by a Tukey's multiple comparisons test was performed. *$P < 0.05$; **$P < 0.01$; ***$P < 0.001$. Amyg, amygdala; Cd, caudate; Ctrl, control; GPe, external globus pallidus; GPi, internal globus pallidus; Hip, hippocampus; Hy, hypothalamus; PrG, precentral gyrus; Put, putamen; StT, nucleus of stria terminalis; Thal, thalamus.

Neurotransmitter and metabolite alterations between non-LID and LID

A thorough comparison of monoamine metabolites between non-LID and LID animals was performed in 18 brain regions (Fig. 2A and fig. S3). There was a significant increase in L-DOPA and 3-OMD in the LID group compared to the non-LID group in all 18 brain regions (Fig. 2, B and C). DA was significantly elevated in LID in all brain regions, except Cd and Put. There was a nonsignificant trend toward increased DA in these regions. The catechol-*O*-methyl transferase (COMT) metabolite of DA, 3-MT, was significantly elevated in the LID state in the following 13 regions: anterior cingulate gyrus (ACgG), claustrum, entorhinal area (Ent), external GP (GPe), internal GP (GPi), hippocampus, insula, inferior temporal gyrus (ITG), middle temporal gyrus (MTG), postcentral gyrus (PoG), PrG, superior temporal gyrus (STG), and thalamus. The monoamine oxidase (MAO) metabolite DOPAC was only significantly elevated in the claustrum, although there was a trend of increased DOPAC throughout the most analyzed regions in LID. These results indicate that the excess DA in LID is preferentially metabolized to 3-MT via COMT.

The $\log_2$ fold change ($\log_2$FC) of L-DOPA levels was highest in GPi and lowest in hypothalamus, ranging from 5 to 7 (Fig. 2B). 3-OMD had a $\log_2$FC of approximately 4 to 5 in all regions. DA was elevated the most in Ent and hippocampus ($\log_2$FC = 3.8, for both). 3-MT displayed the largest increases in GPi ($\log_2$FC = 5.5), hippocampus ($\log_2$FC = 5.3), Ent ($\log_2$FC = 5.6), and thalamus ($\log_2$FC = 4.8). DOPAC was elevated the most in hypothalamus ($\log_2$FC = 2.3), GPi ($\log_2$FC = 2.4), and claustrum ($\log_2$FC = 1.9), although the

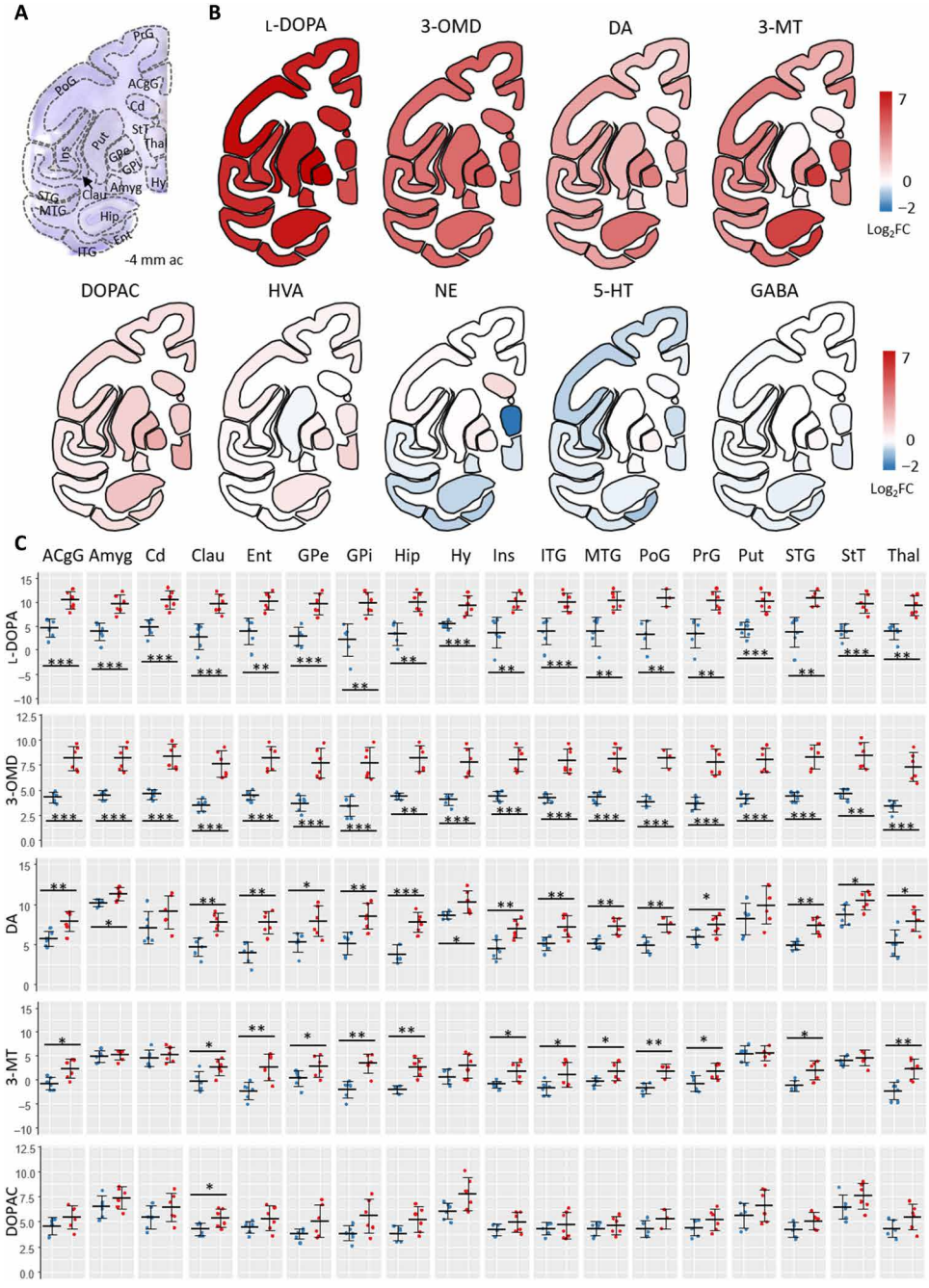

Fig. 2. Regional alterations of metabolites in non-LID versus LID. (**A**) Nissl-stained macaque brain tissue section at −4 mm ac with annotated brain regions. (**B**) Regional heat maps color-coded according to log_2FC between non-LID and LID. Blue indicates elevated levels in non-LID, red indicates higher levels in LID, and white indicates no change. (**C**) Regional quantitation of metabolites in non-LID and LID. Log_2-transformed AUC values for each sample are shown. Blue, non-LID; red, LID. Crossbar and error bars show means and SDs. A Shapiro-Wilk normality test was used to determine normal distribution of samples; a Student's *t* test was used when passing normality test; otherwise, a Mann-Whitney *U* test was used. **P* < 0.05; ***P* < 0.01; ****P* < 0.001. For all metabolites in all regions, *n* = 6, except *n* = 5 for PoG in LID group, *n* = 3 for PoG in non-LID group, and *n* = 5 for Hip in non-LID. Statistical results are summarized in table S2. ac, anterior commissure; ACgG, anterior cingulate gyrus; Clau, claustrum; Ent, entorhinal area; Ins, insula; ITG, inferior temporal gyrus; MTG, middle temporal gyrus; PoG, postcentral gyrus; STG, superior temporal gyrus.

alterations were not significant. Noticeably, the metabolites that occur early in the metabolic pathway, i.e., L-DOPA, 3-OMD, DA and 3-MT, exhibited the greatest changes, whereas the end-metabolite HVA was not significantly altered (Fig. 2 and fig. S3). The animals were euthanized 1 hour after L-DOPA administration, which is enough time for HVA formation according to pharmacokinetic data (*26*), suggesting that there may be a rate-limiting step in HVA formation, possibly due to the extreme levels of L-DOPA in the LID brains. Another possible explanation is that the HVA clearance from the brain is high enough to prevent elevated levels of HVA.

5-HT showed a trend to decrease in LID animals, especially in cortical regions, hippocampus, hypothalamus, and thalamus, indicated by the blue color on the heatmap (Fig. 2B); the difference was, however, not significant. The remaining investigated metabolites GABA, DOPEG, MOPEG, 5-HIAL, 5-HIAA, and taurine did not show any significant difference between non-LID and LID in the investigated regions (fig. S3).

The MALDI-MS images were outlined in a metabolic pathway to visualize the monoaminergic differences between non-LID and LID animals (Fig. 3B). A marked increase in L-DOPA and 3-OMD was obvious in LID animals. DA increased especially in extrastriatal regions, such as cerebral cortex, GP, and hippocampus. The DA metabolites 3-MT, DOPAC, and HVA had highest abundance in the Put, Cd, StT, and hypothalamus. NE was highest in the hypothalamus, StT, and amygdala but was also abundant in cortical regions predominantly in ACgG, PrG, PoG, and insula. GABA was most abundant in both segments of GP but was also abundant throughout the whole gray matter (Fig. 3C). 5-HT was highly abundant in amygdala, hypothalamus, GPi, StT, and medial Cd (Fig. 3D). 5-HIAL had similar distribution as 5-HT; however, 5-HIAA was more abundant throughout the tissue section and, not defined to specific structure to the same extent as 5-HT, with highest intensity detected in hypothalamus, GP, and amygdala (Fig. 3D).

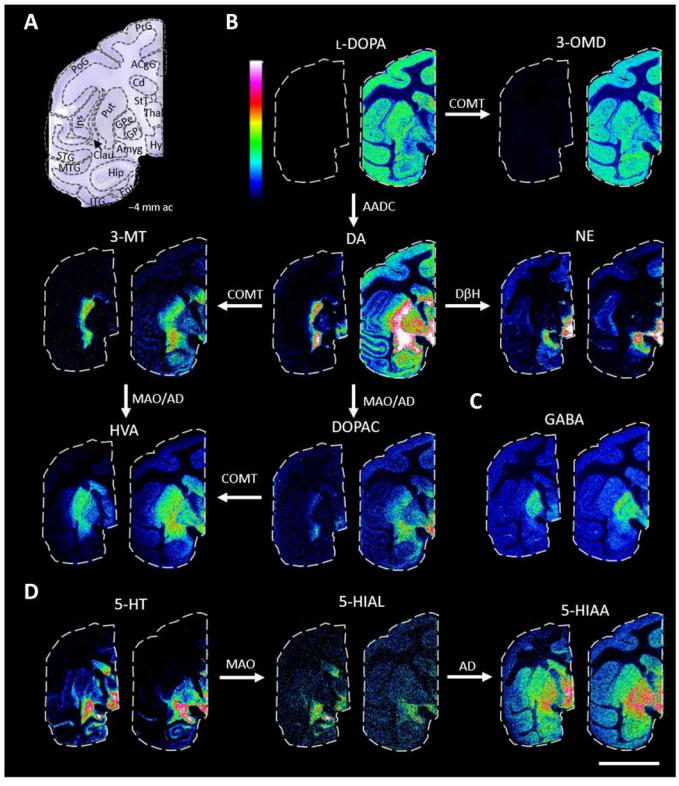

Fig. 3. MALDI-MS images of neurotransmitters and metabolites in non-LID and LID. (**A**) Nissl-stained macaque brain tissue section at −4 mm ac with annotated brain regions. (**B**) Catecholaminergic metabolic pathway. All MALDI-MS images are RMS-normalized and log-transformed intensities. L-DOPA, 3-OMD, 3-MT, HVA, and DOPAC are scaled to 0 to 100% of maximum intensity, and DA and NE are scaled to 0 to 10% of maximum intensity. (**C**) GABA, scaled to 0 to 100% of maximum intensity. (**D**) 5-HT metabolic pathway: 5-HT scaled to 0 to 15%, 5-HIAL scaled to 0 to 20%, and 5-HIAA scaled to 0 to 50% of maximum intensity. For all images: left section, non-LID; right section, LID; scale bar, 20 mm; lateral resolution, 150 μm. Enzymes involved are annotated by the arrows. COMT, catechol-*O*-methyl transferase; MAO, monoamine oxidase; AADC, aromatic L-amino acid decarboxylase; DβH, dopamine-β-hydroxylase; AD, aldehyde dehydrogenase.

Neurotransmitter abundance in control, MPTP, non-LID, and LID animals

To investigate how the levels of metabolites related to control animals and MPTP-exposed animals without L-DOPA treatment, we compared the relative abundance of L-DOPA, NE, 5-HT, and GABA between control, MPTP, non-LID, and LID groups in 10 selected regions: Cd, Put, GPe, GPi, PrG, thalamus, hypothalamus, hippocampus, amygdala, and StT (table S3). We found that L-DOPA levels were equal between non-LID and control animals in the Cd and Put (fig. S4). This may be interpreted as the non-LID animals having had an optimal amount of L-DOPA, whereas LID animals had an overdose of L-DOPA. The MPTP animals had significantly lower L-DOPA in the Cd and Put compared to the other three groups (fig. S4). In the remaining regions, L-DOPA was significantly elevated in LID compared to all other three groups (fig. S4). The MPTP, non-LID, and LID groups had decreased NE levels compared to controls in the Cd and a similar trend was observed in Put, although the decrease was not significant for non-LID and LID groups (fig. S4). 5-HT did not show a significant change between the groups in the brain regions analyzed (fig. S4). GABA was increased in both non-LID and LID compared to the MPTP group in Cd, Put, GPe, GPi, and PrG. In addition, GABA was elevated in non-LID and LID compared to control in the Put (fig. S4). MALDI-MS images of control, MPTP, non-LID, and LID are presented in fig. S2.

Increases of L-DOPA in LID correlated to elevated DA and 3-OMD concentrations

To understand the fate of L-DOPA in the non-LID and LID brains, we investigated the relationships between L-DOPA and its two metabolites 3-OMD and DA with LR analysis, where the levels of metabolites were correlated with their precursor (L-DOPA). Although this analysis cannot prove a causal relationship, we hypothesize that a highly linear relationship would indicate that the formation of the product metabolites, i.e., 3-OMD or DA, was highly dependent on the substrate (L-DOPA) concentration. Any region displaying a signal lower than three times the noise level of the mass spectra was excluded from the analysis. No regions were excluded in the LID groups. However, because of the low intensity of L-DOPA in several non-LID brain regions, the number (n) was reduced to $n = 3$ in hippocampus; $n = 4$ in claustrum, Ent, GPe, GPi; and $n = 5$ in amygdala. In addition, in Ent in non-LID, the number of samples was reduced to $n = 3$ for the correlation of L-DOPA to DA due to low DA levels in three of the samples.

For the COMT metabolite, 3-OMD, there was a significant linear relationship in all regions in the LID group (Fig. 4A), where all fitted models had a similar slope (0.57 to 0.65), indicating a homogeneous rate of formation of 3-OMD in response to increased L-DOPA concentration. In the non-LID group, there was a significant linear relationship in Cd, GPe, Put, StT, and cortical regions (Ctx, Fig. 4). In these brain structures, a lower rate of formation of 3-OMD was found in response to increased L-DOPA levels in the non-LID group, indicated by a reduced slope (0.26 to 0.33).

For the conversion of L-DOPA to DA, there was a significant linear relationship in the LID group in all investigated regions except for the Cd and Put, the main target structures for L-DOPA

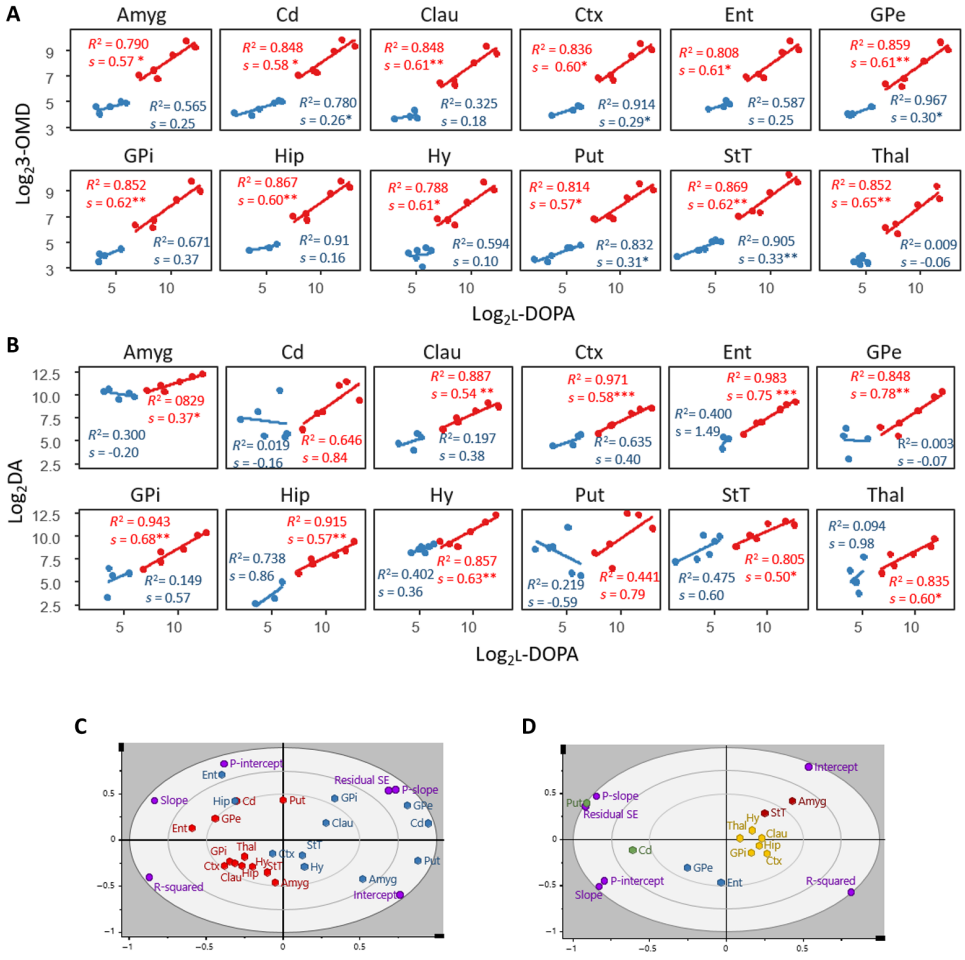

Fig. 4. Correlation of L-DOPA to 3-OMD or DA in non-LID and LID. (**A**) LR of the change in 3-OMD content in response to L-DOPA. (**B**) LR of the change in DA content in response to L-DOPA. (A and B) Blue, non-LID; red, LID. A significant linear relationship is indicated with $*P < 0.05$, $**P < 0.005$, and $***P < 0.001$. For all linear models, $n = 6$ in the LID group, and Cd, Hy, Put, and StT in the non-LID group. For the remaining non-LID regions, $n = 5$ in Amyg and Thal, $n = 4$ in Clau, Ctx, GPe, and GPi, $n = 3$ in Hip in both correlations, $n = 4$ in Ent in L-DOPA to 3-OMD, and $n = 3$ in Ent in L-DOPA to DA. (**C**) PCA model computed from results of LR models in (B); blue, non-LID; red, LID; purple, loadings. (**D**) PCA model computed from results of LR analysis for change in DA in response to increased L-DOPA in LID only. Regions are color-coded according to hierarchical clustering and grouping structures that respond similarly to changes in L-DOPA content. P-intercept, *P* value for intercept; P-slope, *P* value for slope; R-squared, R^2; Residual SE, SE of residuals.

treatment (Fig. 4B). The non-LID group did not have a significant linear relationship between L-DOPA and DA in any structure. Note that the concentration range of L-DOPA was not the same in the two groups, and therefore, it was not appropriate to extrapolate the results from the non-LID to the higher L-DOPA levels. If non-LID animals would have had L-DOPA tissue levels in the same range as the LID animals, they may have shown the same results as LID. The important finding is that the correlations between the levels of L-DOPA and its two metabolites are highly linear when L-DOPA is elevated, as in the LID state.

A principal components analysis (PCA) was performed on the output from the LR analysis: the slope, intercept, *P* value for slope, *P* value for intercept, R^2, and SE of residuals (obtained from LR between L-DOPA and DA). The resulting PCA showed that the brain regions of LID and non-LID were separated, except for the Cd and Put of the LID group that were located closer to the non-LID regions (Fig. 4C). The main separators were the *P* value for the slope, SE of residuals, and R^2, i.e., parameters that describe the linearity of the LR model. To simplify, the groups were separated on whether they had a significant LR or not. To further investigate the response in different brain structures to increased L-DOPA in the LID group, a PCA with only the LID group was performed and a hierarchical clustering analysis grouped structures that responded similarly to changes in L-DOPA content (Fig. 4D). Put and Cd were placed far from the other brain regions because of their high *P* value for slope and SE of residuals, i.e., nonsignificant LR. GPe and Ent are grouped because of their high slope and insignificant intercept, suggesting that their DA levels increased more in response to increased L-DOPA than in other brain structures, and when there is no exogenous L-DOPA present, there is negligible amounts of DA in these structures. Amygdala and StT are grouped because of a high and significant intercept illustrating the high amount of DA present in these structures regardless of the presence of exogenous L-DOPA. Last, hypothalamus, claustrum, thalamus, GPi, hippocampus, and cortical regions are grouped, as their LR models had moderate values for the slope and intercept and a good fit indicated by a high R^2.

Changes in striatal metabolism of DA

We investigated different routes of DA metabolism using the ratios of the MAO metabolite DOPAC and the COMT metabolite 3-MT to DA in the Cd and Put. The DOPAC/DA ratio was not different between the two groups (Fig. 5A). The 3-MT/DA ratio was, however, higher in non-LID than in LID in both Cd and Put (Fig. 5B). Considering the previous analysis, where we found no significant difference in either 3-MT or DA levels in Cd and Put, the difference in 3-MT/DA ratio indicated that there was an altered COMT metabolism between the two groups in the striatal regions, with higher COMT activity in non-LID animals than in LID animals.

Localization of 5-HT, NE, and DA in the striatum and hippocampus

We observed a patchy distribution of DA in non-LID animals. These patches were also found in the striatum at brain levels −4, −2, 0, and +4 mm from the anterior commissure (ac) in non-LID animals (fig. S5). The LID animals did not show such patchy DA distribution but rather a smoother distribution with the highest intensity in the medial part fading into the lateral part of Put. We quantified these patches by counting the number of patches in Cd and Put in each tissue section, and a significantly higher number of patches were observed in non-LID animals (fig. S5). A patchy distribution of NE that colocalized with some of the DA patches (arrows, Fig. 6A) was observed in the Put of non-LID macaque brains.

Serotonergic neurons can uptake exogenous L-DOPA, synthesize, and release DA as a false neurotransmitter and, due to the lack of efficient reuptake capacity, cause fluctuation of extracellular DA, which is one of the most compelling hypotheses explaining LID, based on preclinical and clinical data (*27*). In addition, synaptic 5-HT content may decrease due to its displacement by DA in 5-HT neurons. In the current study, however, quantitation of 5-HT did not show a significant change in 5-HT levels in LID compared to the other investigated groups (fig. S4). We investigated the localization of 5-HT and DA to evaluate the potential formation of DA in 5-HT neurons in striatal structures, Cd and Put, and also in the hippocampus. We found a very low amount of 5-HT in the Put (Fig. 6A), as previously shown (*7*), and its localization could not be correlated with the DA distribution in either non-LID or LID. Overlaying DA and 5-HT distributions showed little concordance of signals in the Put (Fig. 6A), and we were, therefore, unable to show DA displacement in 5-HT neurons in the Put using this approach.

The hippocampus is innervated by serotonergic neurons heterogeneously to different hippocampal layers (*28*). In control animals, we detected 5-HT prominently in the molecular layer of hippocampus (CAml), in the hilar region of the dentate gyrus (HDG), and in stratum radiatum of CA3 and CA1 (CArd) (Fig. 6B). Although carrying a known physiological function (*29*), DA abundance was low in the hippocampus of control animals and was mainly confined to the molecular layer of the dentate gyrus and the outer part of HDG along the surface of the granular layer of the dentate gyrus. In control animals, 5-HT and DA distributions did not overlap. In the LID animals, however, DA was more widely distributed throughout the hippocampus than in control, with high levels in CAml and whole HDG, illustrating overlap with 5-HT, an indication of DA displacement in 5-HT neurons occurring in LID. In contrast, the non-LID animals showed very low abundance of DA not associated with specific hippocampal layers. The localization pattern of NE in hippocampus was similar in all groups.

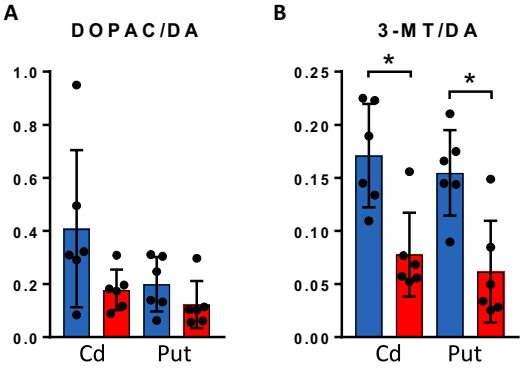

Fig. 5. DA metabolism in striatum. (**A**) DOPAC/DA ratio (MAO metabolism of DA) and (**B**) 3-MT/DA ratio (COMT metabolism of DA) in Cd and Put in non-LID (blue) and LID (red). Bars show means, and error bars show SDs ($n = 6$ for both groups in both regions). A Mann-Whitney *U* test was used; results are summarized in table S4. *$P < 0.05$.

Distribution pattern of DA, 5-HT, and NE in different cerebral cortical areas

Higher-order brain functions are processed in the cerebral cortex and are modulated by the monoaminergic transmission (*30*). We investigated the monoaminergic distribution in the primary motor cortex (PrG), a key region for the execution and control of movement and in the temporal gyrus (TG), involved in sensory processing (Fig. 7A). The monoaminergic neurons innervate cortical areas with laminar specificity (*30*, *31*). In PrG, the DA neurons from the ventral tegmental area mainly innervate deep cortical layers, but the 5-HT neurons from dorsal raphe nucleus and NE neurons from the locus coeruleus innervate layer I with greater density than deep layers (*30*). A laminar distribution was observed for all three neurotransmitters (Fig. 7B). In the PrG, the control had low DA in layer I but high 5-HT, whereas non-LID and LID had high DA in layer I, similar to the 5-HT distribution, indicating that the DA in layer I in non-LID and LID animals originated in 5-HT neurons, another indication of DA displacement in 5-HT neurons. NE had a homogeneous distribution throughout the PrG but was slightly higher in the outer layer in all three states.

In the TG, the three groups had a similar distribution of DA, which was high in the outer layers, low in middle layers, and modest in the deep layers (Fig. 7C). This distribution pattern was similar to previously reported pattern of TH-immunoreactive fibers in the TG, where the highest density was found in layers I and VI (*32*). All animals had high 5-HT and NE in the outer layers of the TG.

The laminar distribution of DA was divided into three layers for relative quantification, namely, outer, middle, and inner layers, containing cortical layers I and II, III and IV, and V and VI, respectively (Fig. 7D). The abundance of DA was significantly elevated in LID in all layers, except in the outer layer of PrG ($P = 0.0815$), although this layer showed a similar trend as the other layers (Fig. 7E). The outer layers displayed the highest DA levels consistently throughout PrG, insula, and the TG (Fig. 7E).

DISCUSSION

Although L-DOPA can cause severe side effects such as LID after long-term treatment, it remains the most effective symptomatic

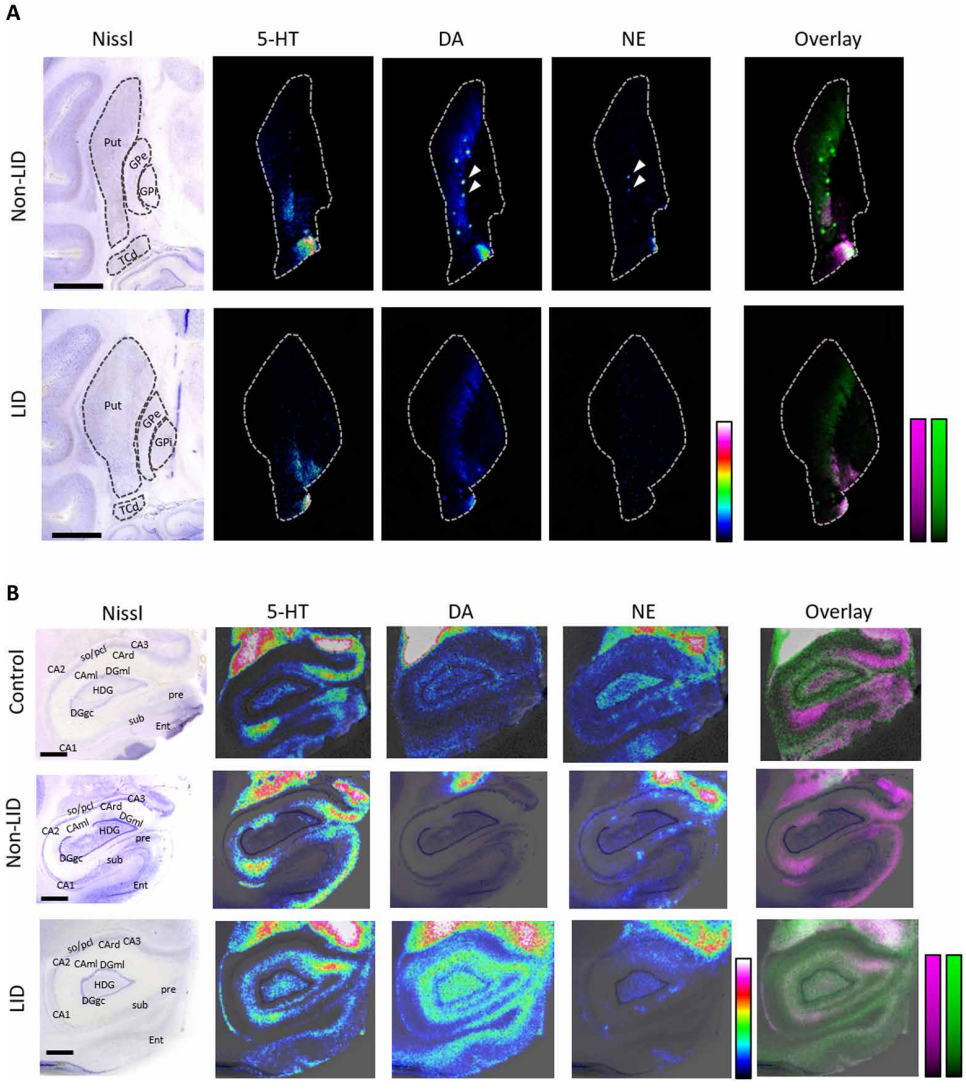

Fig. 6. Comparison of 5-HT, DA, and NE localization in basal ganglia and hippocampus. (**A**) Nissl-stained section showing basal ganglia structures at −6 mm ac and MALDI-MS images of 5-HT (scaled to 0 to 25%), DA (scaled 0 to 30%), and NE (scaled to 0 to 40%) in non-LID and LID. Lateral resolution, 50 μm. Scale bars, 5 mm. White arrows indicate DA and NE patches that colocalize. (**B**) Nissl-stained section of Hip at −4 mm ac and MALDI-MS images of 5-HT, DA, and NE (all scaled to 0 to 20%) in control, non-LID, and LID macaque brain. Lateral resolution, 80 μm. Scale bars, 2 mm. For (A) and (B), images are RMS-normalized and log-transformed, and overlays show DA in green and 5-HT in magenta. CA, Cornu ammonis; CAml, molecular layer of the Hip; CArd, stratum radiatum; DGgc, granular layer of the dentate gyrus; DGml, molecular layer of the dentate gyrus; HDG, hilus of the dentate gyrus; so, stratum oriens; pcl, pyramidal cell layer; pre, presubiculum; sub, subiculum; TCd, tail of caudate nucleus.

therapy for PD (*33*). The rationale of L-DOPA treatment is to increase the striatal DA concentration to compensate for the DA loss following dopaminergic denervation. The mechanisms of L-DOPA's action are, however, not fully understood. Accumulating evidence has shown that L-DOPA affects wide networks of neurotransmitter systems that can be involved in LID and other side effects of L-DOPA treatment (*9*). Although poorly considered, L-DOPA itself has been hypothesized as acting as a neurotransmitter (*34*).

In the present study, we have used our recent advances in the visualization of comprehensive neurotransmitter networks by MALDI-MSI to investigate the relative abundance of multiple neurotransmitters and their metabolites, possibly involved in LID, in specific brain regions (*15*). Through this methodology, we were able to map the brain distribution of L-DOPA, DA, and derived metabolites in a nonhuman primate model of PD and LID. Our results revealed excessive amounts of L-DOPA and 3-OMD in brains of LID animals. All animals received the same dose, 20 mg/kg orally, twice daily for 3 months, with the last dose given 1 hour before euthanasia (*16*, *18*). Despite the fact that striatal L-DOPA was increased more than 30 times in LID compared to non-LID, we did not find a significant rise in DA in the striatum. This unexpected result is contrary to previous studies, performed using microdialysis and positron emission tomography (PET), that have suggested a significant rise in extracellular DA in the striatum associated with LID (*3*, *5*, *8*, *27*). Most of these microdialysis studies have, however, been performed on the 6-hydroxydopamine (6-OHDA)–lesioned rodent model of PD, which does not fully represent the human biology and anatomy as well as the nonhuman primate model. A microdialysis study in

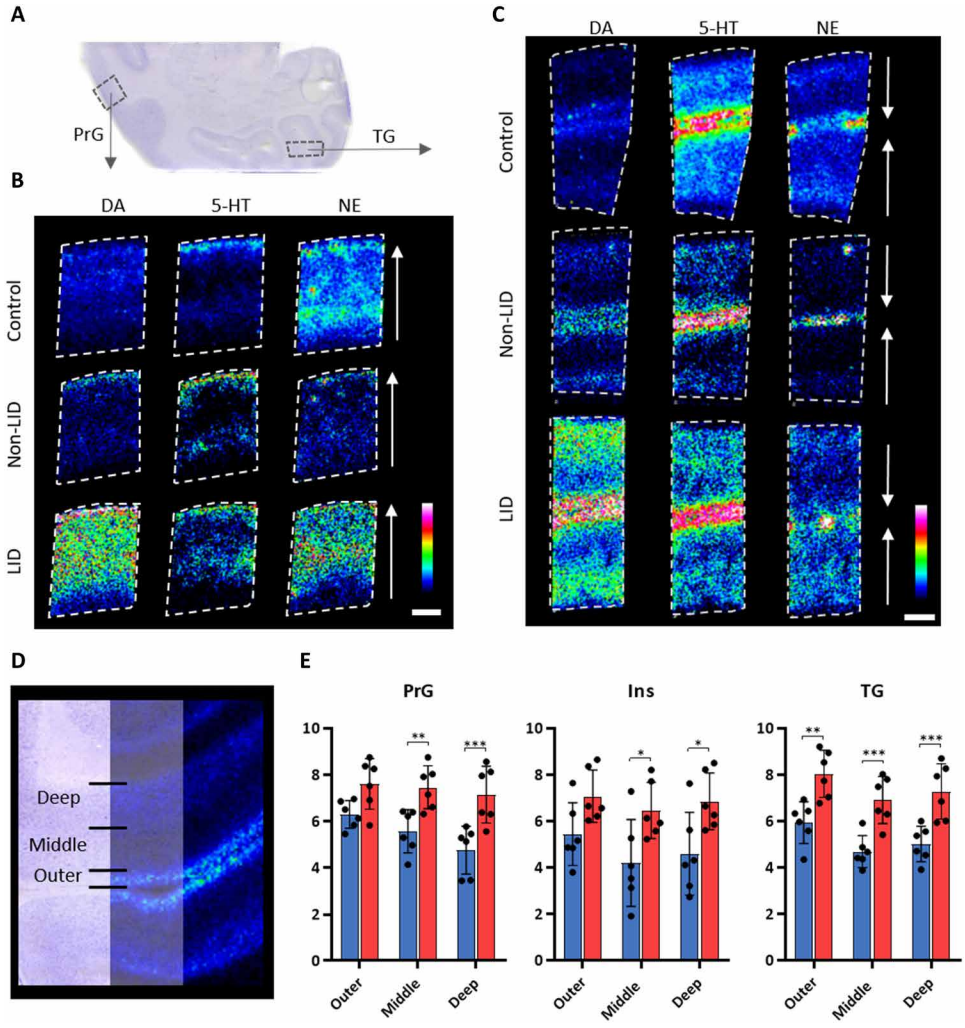

Fig. 7. Mapping of DA throughout cortical areas and layers. (**A**) Nissl-stained coronal tissue section at −4 mm ac illustrating the location of the analyzed cortical area. (**B**) MS images of DA, 5-HT, and NE in PrG and (**C**) TG at −4 mm ac. Color intensity scale is 0 to 50% for DA and 5-HT and 0 to 30% for NE. Lateral resolution, 50 μm; scale bar, 1 mm; images are RMS-normalized. The arrows in (B) and (C) show the orientation of the sample pointing toward the outer layers of the cortex. (**D**) Nissl-stained cortex section overlaid with DA distribution illustrating the three layers of the cortex that were analyzed. (**E**) Relative quantitation of DA in outer, middle, and deep cortical layers at −4 mm ac in the PrG, Ins, and TG. Bars show means, and error bars show SDs; blue, non-LID; red, LID. Statistics were performed using a two-way ANOVA and a post hoc Sidak's multiple comparisons test ($n = 6$ for both groups in all cortical layers). *$P < 0.05$; **$P < 0.01$; ***$P < 0.001$. Two-way ANOVA results are summarized in table S5.

the MPTP primate model did not detect any significant rise in DA in the striatum associated with LID (*10*). In addition, PET measures the changes in L-DOPA–induced displacement of [^{11}C]raclopride binding (*3*, *35*, *36*). Previous reports concluded that such changes reflect changes in synaptic DA levels, based on the assumption that only DA could displace raclopride binding (*3*, *35*, *36*), the possibility of any other endogenous ligand not having been considered. With the method used in the current study, total brain levels were measured and extracellular DA could not be distinguished from intracellular DA. The data, however, raise the possibility that L-DOPA itself may be a contributory factor in causing LID, indicating that stabilization of brain L-DOPA levels is of high importance to prevent dyskinesia. Our results showed that non-LID animals had the same amount of L-DOPA in the striatum as control animals, indicating that non-LID animals had a favorable amount of L-DOPA.

The profuse amount of evidence that has emerged during the past 20 years of a central role of 5-HT system in LID has to be mentioned in this context. Evidence in rodents and nonhuman primates has shown that 5-HT neurons are a significant source of extracellular DA in LID. Lesioning of 5-HT neurons (*5*–*8*) or coadministration of tryptophan with L-DOPA significantly improves or, in some cases, completely abolishes dyskinesia (*37*). In addition, 5-HT$_{1A}$ and 5-HT$_{1B}$ agonists and some serotonin transporter inhibitors are effective antidyskinetic agents, as shown in preclinical and clinical studies [reviewed in (*38*, *39*)]. However, not all data that have been produced in LID research can be fully explained by the ectopic release of DA from serotonergic neurons.

While there is a direct relationship between L-DOPA dose and LID occurrence and severity, some PET studies suggest that LID is not strictly paralleled by a rise in striatal DA tone (*3*). Earlier findings have demonstrated that L-DOPA may act on its own (*40*). L-DOPA produces some pharmacological actions not through conversion to DA (*41*), which suggests antiparkinsonian action of L-DOPA itself shown in both the 6-OHDA–lesioned and reserpine-treated

rat models of PD (*42*, *43*). Such antiparkinson action happened before the elevation in DA when L-DOPA was administered after pretreatment with benserazide or in the absence of DA when L-DOPA was given in combination with NSD-1015, a central AADC inhibitor (*43*). The present results lead us to hypothesize that the antiparkinson effect might be due to either (i) a direct effect of L-DOPA upon supersensitive DA receptors in the absence of the endogenous ligand while striatal levels of L-DOPA are markedly increased, (ii) the action of DA outside the striatum, because there was a significant rise in DA everywhere except in the striatum, or (iii) a combination of both. Such a provocative hypothesis deserves further investigation.

A direct role for L-DOPA upon LID, independently from DA, has received little attention beyond the classic conversion into DA (*44*, *45*). We recently showed that L-DOPA can alter basal ganglia activity and produce LID without enhancing striatal DA release in dyskinetic parkinsonian macaques using microdialysis (*10*). L-DOPA has, however, little affinity for DA receptors. In physiological conditions, DA would compete with and prevent L-DOPA binding to DA receptors. In a condition of depleted DA, it is possible that L-DOPA's affinity for DA receptors is sufficient to enable it to bind to those receptors with physiological effect. In view of the well-documented pathological activation of noncanonical signaling cascades of DA receptors in LID (*4*), one can posit that L-DOPA might actually be a biased agonist to DA receptors, preferentially activating noncanonical cascades leading to LID. While biased agonists aim at dissociating on-target benefits from adverse effects (*46*), we here face a situation where the biased agonist is detrimental.

In the light of fluctuating L-DOPA levels, considerable efforts have been made to stabilize L-DOPA delivery to decrease LID with promising results using intravenous or intestinal infusion (*47*, *48*). It is, however, important to understand the physiological process that leads to the extensive difference in L-DOPA levels in brain tissue between the two states. The plasma and CSF data showed that both non-LID and LID had similar L-DOPA levels, indicating that the large difference we report in brain tissue L-DOPA is not due to peripheral differences. Therefore, the transportation of L-DOPA into the brain might be facilitated in LID animals, causing accumulation of L-DOPA possibly due to blood-brain barrier impairment (*49*, *50*), or L-DOPA may be effluxed in non-LID animals. Such an efflux transporter has been previously characterized and shown to reduce brain bioavailability of L-DOPA (*51*).

The biological effect of 3-OMD has been studied preclinically. Studies in rats have shown that 3-OMD reduced locomotor activity and decreased DA metabolite concentrations (*52*, *53*). When 3-OMD was combined with L-DOPA, the decrease in DA metabolites was reversed. In addition, 3-OMD inhibited the DA transporter but did not bind to DA receptor 1 (*52*). These results suggest a synergistic effect between L-DOPA and 3-OMD in the brain. The coexistence of excessive amounts of L-DOPA and 3-OMD in dyskinetic primate brains could potentially contribute to dyskinesia.

In a previous study that analyzed tissue samples from the same animals as in the present study, the levels of DA, NE, and 5-HT were quantified by HPLC in striatum, motor cortex, amygdala, and hippocampus (*9*). The study reported no significant increase of DA in the striatum in LID compared to non-LID, which is in accordance with our current findings. Similarly, DA was increased in LID compared to controls and non-LID in hippocampus and amygdala (*9*). However, the HPLC analysis reported decreased 5-HT in the striatum, hippocampus, and amygdala in LID compared to controls, in contrast to the present study. In addition, we found that NE was decreased only in the striatum following MPTP treatment (including non-LID and LID) compared to control. The HPLC study did not detect NE in the striatum but reported decreased levels in motor cortex in non-LID compared to control, and in amygdala in non-LID and LID compared to control (*9*).

HPLC has been the mainstay to quantify neurotransmitters in brain tissue but results in the loss of the spatial information from the sample. It merely provides an average concentration of the brain region selected, i.e., it does not resolve intraregional changes of neurotransmitters and metabolites. The approach may also suffer from variable dissection skills. On the other hand, the method may provide a better overall estimate of a concentration of a transmitter in a whole brain region than MALDI-MSI, where often only a single tissue section is analyzed at a certain brain level. Therefore, the levels of the neurotransmitters and metabolites vary depending on the exact localization where the tissue section was collected, and the two methods may therefore not always provide the same results. An advantage of MALDI-MSI is that it enables quantitative analysis in relatively small regions of a tissue sections, which may be very difficult to perform in tissue homogenates using HPLC.

Although MALDI-MSI cannot distinguish extracellular from intracellular metabolite levels, the simultaneous mapping of multiple neurotransmitters and their metabolic pathways has several advantages, besides the number of brain regions and metabolites measured in a single experiment. The formation of DA metabolites can be an indication of the compartmental location of DA. In regions with significantly elevated DA levels, we found mainly increases of the COMT metabolite 3-MT but not of the MAO metabolite DOPAC. 3-MT has been established as an indicator of DA release because of the location of the COMT enzyme (*54*), which indicated that the excess DA was metabolized extraneuronally, and therefore located extraneuronally. We also explored the potential of MALDI-MSI to show DA replacement in 5-HT neurons by comparing distribution patterns of the two neurotransmitters. Our data were not suitable to illustrate this displacement in the striatum, mainly because of the low detection of 5-HT in the striatum. We were, however, successful in showing that 5-HT–rich layers in the hippocampus and in the PrG had increased amount of DA in the dyskinetic animals.

Research on LID has mainly focused on pathophysiological changes in the basal ganglia and motor cortex. However, possible involvement of nonmotor nuclei, including the lateral habenula and the bed nucleus of the StT, in the mechanism of LID has been speculated in recent years (*55*, *56*). In the present study, we show that DA increased linearly with increased L-DOPA levels in extrastriatal regions, indicating the inability of nonstriatal brain regions to regulate the conversion of L-DOPA to DA. The effect of elevated L-DOPA and DA in nonstriatal regions has received little attention previously, but the significant changes seen in our study may have implications for a number of motor and behavioral syndromes.

MALDI-MSI revealed DA patches that occurred repeatedly in the Put of MPTP-exposed and non-LID brains. These patches may represent intact DA terminal collections that may have a role in preventing dyskinesia because they were more prevalent in the non-LID animals. We were not able to correlate these DA patches, with other signals either in our MSI data or in the literature, when searching for a pattern comparable with the patchy distribution of DA.

To summarize, we have thoroughly mapped the distribution of monoamines and their metabolites, in non-LID and LID primate brains, highlighting multiple locations of monoaminergic alterations using MALDI-MSI. L-DOPA was highly elevated in LID animals causing an increase in DA and DA metabolites in extrastriatal structures. In addition, 3-OMD, the main metabolite of L-DOPA, was highly elevated in LID, indicating that dysregulated metabolism of L-DOPA is involved in LID. The high L-DOPA levels in LID resulted in elevated levels of DA in extrastriatal regions, which was predominantly metabolized through COMT. The high abundance of DA in extrastriatal regions may exert biological function by altering signaling throughout the whole brain and resulting in various adverse effects of L-DOPA treatment.

MATERIALS AND METHODS

Materials

Deuterium-labeled standards (GABA-d_6, DA-d_4, 3-MT-d_4, Tyr-d_2, NE-d_6, and L-DOPA-d_3) were obtained from Qmx Laboratories (Thaxted, UK). The derivatization matrix FMP-10 was synthesized in-house as previously reported (*15*). Standards for DA, L-DOPA, 3-OMD, 3-MT, NE, 5-HT, 5-HIAA, and GABA used for MS/MS were purchased from Sigma-Aldrich (Stockholm, Sweden).

Animal experiment

All animal experiments were performed according to the European Communities Council directive of 24 November 1986 (86/609/EEC) revised in 2010 (2010/63/EU) for laboratory animal care in an Association for Assessment and Accreditation of Laboratory Animal Care International-accredited facility after acceptance of study design by the Institute of Lab Animal Science (Chinese Academy of Science, Beijing, China) Institutional Animal Care and Use Committee for experiments on nonhuman primates. A skilled and experienced veterinarian supervised the maintenance and care of animals.

The brain tissues analyzed in the current study were obtained from a previously published biobank (*16*–*18*). The biobank consists of female rhesus monkeys (*Macaca mulatta*, Xierxin, PR of China) of age 5 ± 1 years and mean weight 5.3 ± 0.8 kg. Parkinsonism was induced according to a published procedure (*25*, *57*). Monkeys were given daily injections of MPTP (0.2 mg/kg, intravenously) until stabilization of parkinsonian symptoms. Control animals received vehicle (saline, intravenously) for a comparable amount of time as the MPTP exposure. The degree of parkinsonism was assessed using a clinical rating scale optimized for macaques (*58*). The animals in the MPTP group received no further treatment. Animals receiving chronic L-DOPA treatment (20 mg/kg orally, twice daily) received L-DOPA commencing 3 months after the first day of MPTP treatment. The severity of dyskinesia was assessed using a dyskinesia disability scale during a 3-month treatment period (*59*). On the basis of the rating, animals were assigned to groups, where animals scoring zero were assigned to the non-LID group ($n = 6$ for brain tissue sections analyzed with MALDI-MSI and $n = 4$ for CSF and plasma bioanalysis) and animals scoring above zero were assigned to the LID group ($n = 6$ for brain tissue sections analyzed with MALDI-MSI and $n = 4$ for CSF and plasma bioanalysis). For the chronically L-DOPA–treated groups (non-LID and LID), one last L-DOPA dose was administered 1 hour before euthanizing the animals with an overdose of pentobarbital (150 mg/kg, intravenously). The animals were euthanized 6 months after the initial MPTP exposure (or saline, for control), and the brains were quickly removed and immediately frozen by immersion in isopentane, cooled with dry ice, and stored at −80°C. The time between euthanasia and freezing of the samples was 10 min.

CSF and plasma analysis of L-DOPA levels

Bioanalysis was conducted as previously described (*60*) of separate but parallel prepared groups of non-LID and LID monkeys ($n = 4$ per group). Briefly, blood samples were collected immediately before dosing and at 1 hour after L-DOPA administration, and plasma was immediately separated. Lumbar CSF was collected 1 day before dosing and at 1 hour after L-DOPA. After thawing, 20 µl of plasma or CSF was spiked with 100 µl of 0.4 M perchloric acid and 200 µl of the internal standard solution (3-methyl-DOPA at 0.2 µg/ml in 0.4 M perchloric acid solution). Ten microliters of the supernatant aliquot was then injected into the liquid chromatography (Agilent 1200 RRLC, Agilent Technologies, Santa Clara, CA, USA) MS (LC-MS) system (Agilent 6410B, Agilent Technologies). The LC separations of L-DOPA were achieved using a C18 column (3.5 µm, 2.1 mm × 100 mm, Xterra MS, Waters, Milford, MA, USA). The optimum operating parameters of the electrospray ionization interface in positive mode were as follows: nebulizer, 40 psi; dry gas, 9 liters/min; dry temperature, 350°C; capillary voltage, 4000 V; delta electron multiplier voltage, 300 V. Column eluate was switched 0 to 0.9 min to waste and 0.9 to 3.8 min to the mass spectrometer. Quantitation was achieved using multiple reaction monitoring mode. The precursor–to–product ion transitions were mass/charge ratio (m/z) 198.1 to 152.0 for L-DOPA and m/z 212.1 to 152.0 for 3-methyl-DOPA (fragmentor, 70 V; collision energy, 10 V). The limit of quantitation for L-DOPA was 100 ng/ml.

Experimental design

While designing the experiment, several aspects were considered to minimize the technical variability, which can arise during sample preparation and data acquisition. A standard protocol was used during all sample preparations, and the MALDI-MSI data acquisition method was kept the same in all experiments. Only two brain tissue sections could be analyzed in the same MALDI-MSI experiment because of their large size. Therefore, we analyzed first a batch of non-LID and LID samples by randomly pairing one section from each group. A second batch was analyzed where control and MPTP samples were paired. The time between experiments was kept to a minimum, each experiment lasting on average 32 hours. As a quality control measure, deuterium-labeled standards were spotted in a mixture on the glass slide next to the tissue section. MALDI-MSI data were acquired from these standards both before and after data acquisition from the brain tissue samples. These data were used to evaluate intensity changes over time within acquisitions.

Sample preparation

A mixture of deuterium-labeled standards was prepared with concentration of 2.5 mM for Tyr-d_2, 10 mM for GABA-d_6, and 0.1 mM for DA-d_4, 3-MT-d_4, NE-d_6, and L-DOPA-d_3 in 50% methanol in water. Coronal sections 4 mm posterior to the ac (−4 mm ac) were used for relative quantitation. This level was chosen because of feasibility of studying the following regions of interest: Put, Cd, GP, thalamus, hypothalamus, amygdala, and StT, as well as hippocampus

and eight regions of the cerebral cortex including the PrG that contains the primary motor cortex, PoG, ACgG, insula, TG, and Ent. Samples from −6 mm ac were used as technical replicates. In addition, samples at −2, 0, and +4 mm ac were imaged to visualize further the anterior parts of the striatum. Frozen brains were sectioned at 12 μm thickness on a Leica CM3050S cryostat (Leica Microsystems, Wetzlar, Germany) at −20°C, thaw-mounted onto indium tin oxide–coated glass slides (Bruker Daltonics, Bremen, Germany), and stored at −80°C before analysis. On the day of analysis, samples were brought to room temperature in a desiccator. After 30 min in the desiccator, the deuterium-labeled standard solution was spotted on the glass slide (two spots, 0.2 μl) next to the tissue section for quality control. The on-tissue derivatization was performed according to a published protocol (*15*). Briefly, a solution with concentration (1.8 mg/ml) of FMP-10 in 70% acetonitrile was sprayed over the tissue sections with a robotic sprayer (TM-Sprayer, HTX-Technologies). Parameters of the spraying method were as follows: temperature, 80°C; flow rate, 80 μl/min; nozzle velocity, 1100 mm/min; track spacing, 2.0 mm; N2 pressure, 6 psi; number of passes, 30. After matrix application, the two slides were put in a MALDI slide adapter (Bruker Daltonics, Bremen) and scanned using a flatbed optical scanner (Epson Perfection V500, Japan).

Data acquisition

All MSI experiments were carried out on a MALDI-FTICR MS instrument (Solarix 7T-2ω, Bruker Daltonics). Before analysis, the method was calibrated with red phosphorus. Mass range scanned was *m*/*z* 150 to 1500, and Q1 mass was set to *m*/*z* 378. Transient size of 2M and quadrature phase detection of 2ω were used to achieve the minimum acquisition time with sufficient mass resolution. The time-of-flight value was set to 0.700 ms, and transfer optics frequency was 4 MHz. The small laser was used, and spectra were collected by firing 100 shots per pixel. Samples were run at 150-μm lateral resolution for relative quantitation in positive ion mode. Online calibration was performed using *m*/*z* 555.2231, an abundant ion cluster signal of FMP-10. Additional experiments were performed at higher lateral resolution varying from 50 to 80 μm for certain brain areas. These included either samples that were rerun from previous experiment or samples at other coronal brain levels.

Identification of metabolites

Accurate mass was used for identification in addition to on-plate standards and on-tissue MS/MS for metabolites with high enough signal and mass resolution to be isolated and fragmented. The MS/MS spectra from standards were compared to MS/MS spectra obtained from tissue using DataAnalysis (Bruker Daltonics, Bremen, v.4.2). An optimal fragmentation energy was adjusted for each compound, and a blank sample was collected as a negative control to identify fragments matching between standards and tissue. In addition, the metabolites were identified by their anatomical distribution. Furthermore, because multiple signals can arise from a single metabolite, depending on the metabolite's ability to be derivatized (number of primary amines and/or phenol groups), all possible signals form each metabolite were evaluated, considering possible overlapping signals and their signal-to-noise values (*15*).

Data processing

Data were initially visualized in flexImaging (Bruker Daltonics, Bremen, v.5.0). For relative quantitation, all experiments were imported into SCiLS Lab (Bruker Daltonics, Bremen, v.2019c Pro) and merged into a single file. An initial dataset including only non-LID and LID was created for extensive investigation of the differences between these two groups in 18 brain regions. Later, a dataset including all four experimental groups—control, MPTP, non-LID, and LID—was created for investigation of 10 regions. Import parameters were as follows: axis interpolation mode was exponential, and average data point accuracy was 0.60 mDa, leading to a number of 2.249.159 resulting data points.

To explore the technical variability and presence of possible outliers in the non-LID and LID data, a mass list with the 2488 most intense peaks was exported through the report table function in SCiLS Lab. Area under curve (AUC) and maximum intensity values were extracted, both without normalization and normalized to root mean square (RMS) of all data points. These data were used to investigate technical variability with PCA (fig. S6; SIMCA, v.15, Sartorius Stedim Biotech, Umeå, Sweden) and boxplots (RStudio, v.1.1.383, RStudio Team, Boston, MA, USA). This mass list was also used to calculate coefficient of variation for every sample in the non-LID and LID groups.

A separate SCiLS file was created from the data acquired from the deuterated standards run before and after acquisition of tissue samples. The processing parameters were the same as for the tissue experiments: average data point accuracy 0.60 mDa and 2.249.159 resulting data points. Ion signals arising from the deuterated standards were used to evaluate intensity changes over time and between experiments performed on non-LID and LID samples (fig. S7).

Statistical analysis

Student's *t* test was used to compare plasma and CSF concentrations between groups. The correlation between plasma and CSF samples was calculated with LR passing through the origin, and coefficients of determination were calculated to quantify the strength of the relationship between the variables (GraphPad Prism v.8.4, GraphPad Software, La Jolla, CA, USA).

Brain regions were annotated in SCiLS Lab according to a macaque brain atlas (*61*). The 14 targeted metabolites were manually peak-picked (table S1). RMS-normalized AUC values were exported from SCiLS Lab via the report table function and $\log_2$-transformed for all metabolites in all brain regions for relative quantitation.

A sample was considered an outlier if the mean of the sample was outside the average interquartile range of all samples. No whole sample was excluded (fig. S8). However, because of differences between individual brain sections, some regions were not present on all tissue sections, reducing the number (*n*) in the statistical analysis in the following brain areas: hippocampus in non-LID, $n = 5$; PoG in non-LID, $n = 3$; PoG in LID, $n = 5$. A Shapiro-Wilk normality test was performed to determine whether to use a parametric or nonparametric hypothesis test. A Student's *t* test or nonparametric Mann-Whitney *U* test was performed to test for differences between non-LID and LID in 18 brain regions; α of 0.05 was used (SPSS, IBM, Armok, v.22.0). A one-way analysis of variance (ANOVA) with a Tukey's multiple comparisons post hoc test was used to compare all four groups (control, MPTP, non-LID, and LID) in RStudio. Log_2FC was calculated as the $\log_2$ of the ratio (metabolite AUC in LID)/(metabolite AUC in non-LID), and the color scale was created in Excel.

LR analysis was computed in RStudio. AUC values were $\log_2$-transformed to obtain normality. Metabolites in particular brain

regions were excluded if the signal of a metabolite had lower intensity than three times the noise level of the mass spectrum. PCA of the output from the LR was computed in SIMCA where the input was, the slope, intercept, P value for slope, P value for intercept, R^2, and SE of residuals. For relative quantitation of DA in outer, middle, and deep cortical layers, statistical analysis was performed using a two-way ANOVA and a post hoc Sidak's multiple comparisons test ($n = 6$ for both groups in all cortical layers) in GraphPad Prism 8.4.

SUPPLEMENTARY MATERIALS

Supplementary material for this article is available at http://advances.sciencemag.org/cgi/content/full/7/2/eabe5948/DC1

View/request a protocol for this paper from *Bio-protocol*.

REFERENCES AND NOTES

1. J. E. Ahlskog, M. D. Muenter, Frequency of levodopa-related dyskinesias and motor fluctuations as estimated from the cumulative literature. *Mov. Disord.* **16**, 448–458 (2001).
2. M. Politis, K. Wu, C. Loane, D. J. Brooks, L. Kiferle, F. E. Turkheimer, P. Bain, S. Molloy, P. Piccini, Serotonergic mechanisms responsible for levodopa-induced dyskinesias in Parkinson's disease patients. *J. Clin. Invest.* **124**, 1340–1349 (2014).
3. R. de la Fuente-Fernandez, V. Sossi, Z. Huang, S. Furtado, J.-Q. Lu, D. B. Calne, T. J. Ruth, A. J. Stoessl, Levodopa-induced changes in synaptic dopamine levels increase with progression of Parkinson's disease: Implications for dyskinesias. *Brain* **127**, 2747–2754 (2004).
4. M. F. Bastide, W. G. Meissner, B. Picconi, S. Fasano, P. O. Fernagut, M. Feyder, V. Francardo, C. Alcacer, Y. Ding, R. Brambilla, G. Fisone, A. J. Stoessl, M. Bourdenx, M. Engeln, S. Navailles, P. De Deurwaerdere, W. K. Ko, N. Simola, M. Morelli, L. Groc, M. C. Rodriguez, E. V. Gurevich, M. Quik, M. Morari, M. Mellone, F. Gardoni, E. Tronci, D. Guehl, F. Tison, A. R. Crossman, U. J. Kang, K. Steece-Collier, S. Fox, M. Carta, M. A. Cenci, E. Bezard, Pathophysiology of L-dopa-induced motor and non-motor complications in Parkinson's disease. *Prog. Neurobiol.* **132**, 96–168 (2015).
5. H. Tanaka, K. Kannari, T. Maeda, M. Tomiyama, T. Suda, M. Matsunaga, Role of serotonergic neurons in L-DOPA-derived extracellular dopamine in the striatum of 6-OHDA-lesioned rats. *Neuroreport* **10**, 631–634 (1999).
6. M. Carta, T. Carlsson, D. Kirik, A. Björklund, Dopamine released from 5-HT terminals is the cause of L-DOPA-induced dyskinesia in parkinsonian rats. *Brain* **130**, 1819–1833 (2007).
7. D. Rylander, M. Parent, S. S. O'Sullivan, S. Dovero, A. J. Lees, E. Bezard, L. Descarries, M. A. Cenci, Maladaptive plasticity of serotonin axon terminals in levodopa-induced dyskinesia. *Ann. Neurol.* **68**, 619–628 (2010).
8. M. Beaudoin-Gobert, J. Epinat, E. Météreau, S. Duperrier, S. Neumane, B. Ballanger, F. Lavenne, F. Liger, C. Tourvielle, F. Bonnefoi, N. Costes, D. L. Bars, E. Broussolle, S. Thobois, L. Tremblay, V. Sgambato-Faure, Behavioural impact of a double dopaminergic and serotonergic lesion in the non-human primate. *Brain* **138**, 2632–2647 (2015).
9. M. Engeln, P. De Deurwaerdere, Q. Li, E. Bezard, P. O. Fernagut, Widespread monoaminergic dysregulation of both motor and non-motor circuits in parkinsonism and dyskinesia. *Cereb. Cortex* **25**, 2783–2792 (2015).
10. G. Porras, P. De Deurwaerdere, Q. Li, M. Marti, R. Morgenstern, R. Sohr, E. Bezard, M. Morari, W. G. Meissner, L-dopa-induced dyskinesia: Beyond an excessive dopamine tone in the striatum. *Sci. Rep.* **4**, 3730 (2014).
11. A. Chagraoui, M. Boulain, L. Juvin, Y. Anouar, G. Barrière, P. Deurwaerdère, L-DOPA in Parkinson's disease: Looking at the "false" neurotransmitters and their meaning. *Int. J. Mol. Sci.* **21**, 294 (2019).
12. M. Shariatgorji, A. Nilsson, R. J. A. Goodwin, P. Kallback, N. Schintu, X. Q. Zhang, A. R. Crossman, E. Bezard, P. Svenningsson, P. E. Andren, Direct targeted quantitative molecular imaging of neurotransmitters in brain tissue sections. *Neuron* **84**, 697–707 (2014).
13. M. Shariatgorji, P. Svenningsson, P. E. Andrén, Mass spectrometry imaging, an emerging technology in neuropsychopharmacology. *Neuropsychopharmacology* **39**, 34–49 (2014).
14. J. L. Norris, R. M. Caprioli, Analysis of tissue specimens by matrix-assisted laser desorption/ionization imaging mass spectrometry in biological and clinical research. *Chem. Rev.* **113**, 2309–2342 (2013).
15. M. Shariatgorji, A. Nilsson, E. Fridjonsdottir, T. Vallianatou, P. Källback, L. Katan, J. Sävmarker, I. Mantas, X. Zhang, E. Bezard, P. Svenningsson, L. R. Odell, P. E. Andrén, Comprehensive mapping of neurotransmitter networks by MALDI-MS imaging. *Nat. Methods* **16**, 1021–1028 (2019).
16. E. Santini, V. Sgambato-Faure, Q. Li, M. Savasta, S. Dovero, G. Fisone, E. Bezard, Distinct changes in cAMP and extracellular signal-regulated protein kinase signalling in L-DOPA-induced dyskinesia. *PLOS ONE* **5**, e12322 (2010).
17. G. Porras, A. Berthet, B. Dehay, Q. Li, L. Ladepeche, E. Normand, S. Dovero, A. Martinez, E. Doudnikoff, M.-L. Martin-Négrier, Q. Chuan, B. Bloch, D. Choquet, E. Boué-Grabot, L. Groc, E. Bezard, PSD-95 expression controls L-DOPA dyskinesia through dopamine D1 receptor trafficking. *J. Clin. Invest.* **122**, 3977–3989 (2012).
18. P. O. Fernagut, Q. Li, S. Dovero, P. Chan, T. Wu, P. Ravenscroft, M. Hill, Z. Chen, E. Bezard, Dopamine transporter binding is unaffected by L-DOPA administration in normal and MPTP-treated monkeys. *PLOS ONE* **5**, e14053 (2010).
19. G. Porras, Q. Li, E. Bezard, Modeling Parkinson's disease in primates: The MPTP model. *Cold Spring Harb. Perspect. Med.* **2**, a009308 (2012).
20. C. Guigoni, S. Dovero, I. Aubert, Q. Li, B. H. Bioulac, B. Bloch, E. V. Gurevich, C. E. Gross, E. Bezard, Levodopa-induced dyskinesia in MPTP-treated macaques is not dependent on the extent and pattern of nigrostrial lesioning. *Eur. J. Neurosci.* **22**, 283–287 (2005).
21. W. K. D. Ko, S. M. Camus, Q. Li, J. Yang, S. McGuire, E. Y. Pioli, E. Bezard, An evaluation of istradefylline treatment on Parkinsonian motor and cognitive deficits in 1-methyl-4-phenyl-1,2,3,6-tetrahydropyridine (MPTP)-treated macaque models. *Neuropharmacology* **110**, 48–58 (2016).
22. N. M. Urs, S. Bido, S. M. Peterson, T. L. Daigle, C. E. Bass, R. R. Gainetdinov, E. Bezard, M. G. Caron, Targeting β-arrestin2 in the treatment of L-DOPA–induced dyskinesia in Parkinson's disease. *Proc. Natl. Acad. Sci. U.S.A.* **112**, E2517–E2526 (2015).
23. E. Bezard, E. Tronci, E. Y. Pioli, Q. Li, G. Porras, A. Björklund, M. Carta, Study of the antidyskinetic effect of eltoprazine in animal models of levodopa-induced dyskinesia. *Mov. Disord.* **28**, 1088–1096 (2013).
24. M. R. Ahmed, A. Berthet, E. Bychkov, G. Porras, Q. Li, B. H. Bioulac, Y. T. Carl, B. Bloch, S. Kook, I. Aubert, S. Dovero, E. Doudnikoff, V. V. Gurevich, E. V. Gurevich, E. Bezard, Lentiviral overexpression of GRK6 alleviates L-Dopa–induced dyskinesia in experimental Parkinson's disease. *Sci. Transl. Med.* **2**, 28ra28 (2010).
25. E. Bezard, S. Dovero, C. Prunier, P. Ravenscroft, S. Chalon, D. Guilloteau, A. R. Crossman, B. Bioulac, J. M. Brotchie, C. E. Gross, Relationship between the appearance of symptoms and the level of nigrostriatal degeneration in a progressive 1-methyl-4-phenyl-1,2,3,6-tetrahydropyridine-lesioned macaque model of Parkinson's disease. *J. Neurosci.* **21**, 6853–6861 (2001).
26. P. G. Ravenstijn, H. J. Drenth, M. J. O'Neill, M. Danhof, E. C. de Lange, Evaluation of blood-brain barrier transport and CNS drug metabolism in diseased and control brain after intravenous L-DOPA in a unilateral rat model of Parkinson's disease. *Fluids Barriers CNS* **9**, 4 (2012).
27. S. Navailles, B. Bioulac, C. Gross, P. De Deurwaerdere, Serotonergic neurons mediate ectopic release of dopamine induced by L-DOPA in a rat model of Parkinson''s disease. *Neurobiol. Dis.* **38**, 136–143 (2010).
28. C. Köhler, H. Steinbusch, Identification of serotonin and non-serotonin-containing neurons of the mid-brain raphe projecting to the entorhinal area and the hippocampal formation. A combined immunohistochemical and fluorescent retrograde tracing study in the rat brain. *Neuroscience* **7**, 951–975 (1982).
29. L. Ladepeche, J. P. Dupuis, D. Bouchet, E. Doudnikoff, L. Yang, Y. Campagne, E. Bézard, E. Hosy, L. Groc, Single-molecule imaging of the functional crosstalk between surface NMDA and dopamine D1 receptors. *Proc. Natl. Acad. Sci. U.S.A.* **110**, 18005–18010 (2013).
30. C. Vitrac, M. Benoit-Marand, Monoaminergic modulation of motor cortex function. *Front. Neural Circuits* **11**, 72 (2017).
31. S. N. Jacob, H. Nienborg, Monoaminergic neuromodulation of sensory processing. *Front. Neural Circuits* **12**, 51 (2018).
32. D. A. Lewis, M. J. Campbell, S. L. Foote, M. Goldstein, J. H. Morrison, The distribution of tyrosine hydroxylase-immunoreactive fibers in primate neocortex is widespread but regionally specific. *J. Neurosci.* **7**, 279–290 (1987).
33. R. Katzenschlager, A. J. Lees, Treatment of Parkinson's disease: Levodopa as the first choice. *J. Neurol.* **249** (Suppl 2), II19–II24 (2002).
34. Y. Misu, Y. Goshima, T. Miyamae, Is DOPA a neurotransmitter? *Trends Pharmacol. Sci.* **23**, 262–268 (2002).
35. R. de la Fuente-Fernández, J. Q. Lu, V. Sossi, S. Jivan, M. Schulzer, J. E. Holden, C. S. Lee, T. J. Ruth, D. B. Calne, A. J. Stoessl, Biochemical variations in the synaptic level of dopamine precede motor fluctuations in Parkinson's disease: PET evidence of increased dopamine turnover. *Ann. Neurol.* **49**, 298–303 (2001).
36. N. Pavese, A. H. Evans, Y. F. Tai, G. Hotton, D. J. Brooks, A. J. Lees, P. Piccini, Clinical correlates of levodopa-induced dopamine release in Parkinson disease: A PET study. *Neurology* **67**, 1612–1617 (2006).
37. W. K. Ko, Q. Li, E. Bezard, Effects of L-tryptophan on L-DOPA-induced dyskinesia in the L-methyl-4-phenyl-1,2,3,6-tetrahydropyridine (MPTP)-treated macaque model of Parkinson's disease. *Neurosci. Lett.* **566**, 72–76 (2014).
38. P. Huot, S. H. Fox, J. M. Brotchie, The serotonergic system in Parkinson's disease. *Prog. Neurobiol.* **95**, 163–212 (2011).

39. P. Huot, S. H. Fox, J. M. Brotchie, Monoamine reuptake inhibitors in Parkinson's disease. *Parkinsons Dis.* **2015**, 609428 (2015).
40. Y. Misu, Y. Goshima, H. Ueda, H. Okamura, Neurobiology of L-DOPAergic systems. *Prog. Neurobiol.* **49**, 415–454 (1996).
41. Y. Goshima, T. Kubo, Y. Misu, Biphasic actions of L-DOPA on the release of endogenous noradrenaline and dopamine from rat hypothalamic slices. *Br. J. Pharmacol.* **89**, 229–234 (1986).
42. A. Alachkar, J. M. Brotchie, O. T. Jones, Locomotor response to L-DOPA in reserpine-treated rats following central inhibition of aromatic L-amino acid decarboxylase: Further evidence for non-dopaminergic actions of L-DOPA and its metabolites. *Neurosci. Res.* **68**, 44–50 (2010).
43. T. Nakazato, A. Akiyama, Effect of exogenous L-dopa on behavior in the rat: An in vivo voltammetric study. *Brain Res.* **490**, 332–338 (1989).
44. K. Buck, B. Ferger, Comparison of intrastriatal administration of noradrenaline and L-DOPA on dyskinetic movements: A bilateral reverse in vivo microdialysis study in 6-hydroxydopamine-lesioned rats. *Neuroscience* **159**, 16–20 (2009).
45. K. Buck, P. Voehringer, B. Ferger, Site-specific action of L-3,4-dihydroxyphenylalanine in the striatum but not globus pallidus and substantia nigra pars reticulata evokes dyskinetic movements in chronic L-3,4-dihydroxyphenylalanine-treated 6-hydroxydopamine-lesioned rats. *Neuroscience* **166**, 355–358 (2010).
46. J. D. Violin, A. L. Crombie, D. G. Soergel, M. W. Lark, Biased ligands at G-protein-coupled receptors: Promise and progress. *Trends Pharmacol. Sci.* **35**, 308–316 (2014).
47. M. Buongiorno, F. Antonelli, A. Camara, V. Puente, O. de Fabregues-Nebot, J. Hernandez-Vara, M. Calopa, B. Pascual-Sedano, A. Campolongo, F. Valldeoriola, E. Tolosa, J. Kulisevsky, M. J. Martí, Long-term response to continuous duodenal infusion of levodopa/carbidopa gel in patients with advanced Parkinson disease: The Barcelona registry. *Parkinsonism Relat. Disord.* **21**, 871–876 (2015).
48. D. Nyholm, H. Askmark, C. Gomes-Trolin, T. Knutson, H. Lennernas, C. Nyström, S.-M. Aquilonius, Optimizing levodopa phannacokinetics: Intestinal infusion versus oral sustained-release tablets. *Clin. Neuropharmacol.* **26**, 156–163 (2003).
49. R. P. Lerner, V. Francardo, K. Fujita, Z. Bimpisidis, V. A. Jourdain, C. C. Tang, S. L. Dewey, T. Chaly, M. A. Cenci, D. Eidelberg, Levodopa-induced abnormal involuntary movements correlate with altered permeability of the blood-brain-barrier in the basal ganglia. *Sci. Rep.* **7**, 16005 (2017).
50. J. E. Westin, H. S. Lindgren, J. Gardi, J. R. Nyengaard, P. Brundin, P. Mohapel, M. A. Cenci, Endothelial proliferation and increased blood–brain barrier permeability in the basal ganglia in a rat model of 3,4-dihydroxyphenyl-L-alanine-induced dyskinesia. *J. Neurosci.* **26**, 9448–9461 (2006).
51. R. A. Hawkins, A. Mokashi, I. A. Simpson, An active transport system in the blood–brain barrier may reduce levodopa availability. *Exp. Neurol.* **195**, 267–271 (2005).
52. E.-S. Lee, H. Chen, J. King, C. Charlton, The role of 3-*O*-methyldopa in the side effects of L-dopa. *Neurochem. Res.* **33**, 401–411 (2008).
53. Y. Onzawa, Y. Kimura, K. Uzuhashi, M. Shirasuna, T. Hirosawa, T. Taogoshi, K. Kihira, Effects of 3-*O*-methyldopa, L-3,4-dihydroxyphenylalanine metabolite, on locomotor activity and dopamine turnover in rats. *Biol. Pharm. Bull.* **35**, 1244–1248 (2012).
54. B. H. C. Westerink, Sequence and significance of dopamine metabolism in the rat brain. *Neurochem. Int.* **7**, 221–227 (1985).
55. M. F. Bastide, B. de la Crompe, E. Doudnikoff, P.-O. Fernagut, C. E. Gross, N. Mallet, T. Boraud, E. Bézard, Inhibiting lateral habenula improves L-DOPA–induced dyskinesia. *Biol. Psychiatry* **79**, 345–353 (2016).
56. M. F. Bastide, C. Glangetas, E. Doudnikoff, Q. Li, M. Bourdenx, P. O. Fernagut, E. C. Dumont, F. Georges, E. Bezard, Involvement of the bed nucleus of the stria terminalis in L-Dopa induced dyskinesia. *Sci. Rep.* **7**, 2348 (2017).
57. E. Bezard, C. Imbert, X. Deloire, B. Bioulac, C. E. Gross, A chronic MPTP model reproducing the slow evolution of Parkinson's disease: Evolution of motor symptoms in the monkey. *Brain Res.* **766**, 107–112 (1997).
58. C. Imbert, E. Bezard, S. Guitraud, T. Boraud, C. E. Gross, Comparison of eight clinical rating scales used for the assessment of MPTP-induced parkinsonism in the Macaque monkey. *J. Neurosci. Methods* **96**, 71–76 (2000).
59. S. H. Fox, T. H. Johnston, Q. Li, J. Brotchie, E. Bezard, A critique of available scales and presentation of the non-human primate dyskinesia rating scale. *Mov. Disord.* **27**, 1373–1378 (2012).
60. T. Thiollier, C. Wu, H. Contamin, Q. Li, J. Zhang, E. Bezard, Permeability of blood–brain barrier in macaque model of 1-methyl-4-phenyl-1,2,3,6-tetrahydropyridine-induced Parkinson disease. *Synapse* **70**, 231–239 (2016).
61. R. F. Martin, D. M. Bowden, A stereotaxic template atlas of the macaque brain for digital imaging and quantitative neuroanatomy. *Neuroimage* **4**, 119–150 (1996).

Acknowledgments

Funding: This work was financially supported by the Swedish Research Council (Medicine and Health, 2018-03320, and Natural and Engineering Science, 2018-05501), ARIADME, European Community's Seventh Framework Program (FP7 ITN, grant agreement 607517), the Swedish Brain Foundation (FO2018-0292), the Swedish Foundation for Strategic Research (RIF14-0078), the Science for Life Laboratory (all to P.E.A.), Agence Nationale de la Recherche grants ANR-07-MNP TRAFINLID and ANR-08-MNP-018 MCHPRIMAPARK, a Federation pour la Recherche sur le Cerveau grant, and Biothèque Primate—CNRS Life Sciences Department (all to E.B.). **Author contributions:** E.F. conceived the study, designed experiments, acquired data, performed statistical analysis, interpreted results, and wrote the manuscript. R.S. and A.N. conceived the study, designed experiments, acquired and interpreted data, and edited the manuscript. T.V. analyzed data and edited the manuscript. L.R.O. and L.S.S. synthesized the reactive MALDI-MSI matrices. P.S. interpreted results and edited the manuscript. P.-O.F. and E.B. designed and supervised the animal experiments, provided tissue samples, and edited and wrote the manuscript. A.R.C. designed the animal experiments and edited the manuscript. P.E.A. conceived the study, designed experiments, interpreted data, wrote the manuscript, and was the principal investigator for the grants that fund this research. **Competing interests:** The authors declare that they have no competing interests. **Data and materials availability:** The MALDI-MSI data that support the findings of this study are available from the corresponding author upon reasonable request. MS/MS spectra area available in the Supplementary Materials. Source data for all statistical analyses are available online.

Submitted 1 September 2020
Accepted 10 November 2020
Published 6 January 2021
10.1126/sciadv.abe5948

Citation: E. Fridjonsdottir, R. Shariatgorji, A. Nilsson, T. Vallianatou, L. R. Odell, L. S. Schembri, P. Svenningsson, P.-O. Fernagut, A. R. Crossman, E. Bezard, P. E. Andrén, Mass spectrometry imaging identifies abnormally elevated brain L-DOPA levels and extrastriatal monoaminergic dysregulation in L-DOPA–induced dyskinesia. *Sci. Adv.* **7**, eabe5948 (2021).